J Solid State Electrochem (2011) 15:175–182
DOI 10.1007/s10008-010-1087-8

ORIGINAL PAPER

Charge storage performance of doped carbons prepared from polyaniline for supercapacitors

Limin Li · Enhui Liu · Haijie Shen · Yanjing Yang · Zhengzheng Huang · Xiaoxia Xiang · Yingying Tian

Received: 2 March 2010 / Revised: 22 April 2010 / Accepted: 23 April 2010 / Published online: 13 May 2010

Abstract Doped carbons have been prepared from polyaniline for supercapacitors. The morphology of samples has been characterized by scanning electron microscope, the surface chemical composition of samples has been investigated by X-ray photoelectron spectroscopy, and the surface area of samples has been calculated by Brunauer–Emmett–Teller measurement. Electrochemical properties have been studied by cyclic voltammograms, galvanostatic charge/discharge, and electrochemical impedance spectroscopy measurements in 6 mol L^{-1} potassium hydroxide. Their charge storage performance has been evaluated, and the effect of nitrogen atomic functionalities on the pseudocapacitive property has been studied. The experimental results have proved two mechanisms of energy storage in doped carbons: double-layer formation and pseudocapacitance. The overall specific capacitance of doped unactivated carbon is mainly attributed to pseudocapacitance, that of doped activated carbon prepared by physical activation is attributed to the synergic effect of pseudocapacitance and double-layer capacitance, but that of doped activated carbon prepared by chemical activation is mainly attributed to double-layer capacitance.

Keywords Doped activated carbon · Nitrogen functionalities · X-ray photoelectron spectroscopy · Electrochemical properties

L. Li · E. Liu (✉) · H. Shen · Y. Yang · Z. Huang · X. Xiang · Y. Tian
Key Laboratory of Environmentally Friendly Chemistry and Applications of Ministry of Education, College of Chemistry, Xiangtan University,
Hunan 411105, People's Republic of China
e-mail: liuenhui99@sina.com.cn

Introduction

Supercapacitors are promising high power energy sources for many different applications such as hybrid electrical vehicles, pulsed laser system and so on, because of their high power density and long cycle life [1, 2]. Among various electrode candidates for supercapacitors, activated carbons are mostly investigated due to their advantages such as well-developed microstructure, good conductivity, excellent physico-chemical stability, and cost-effectiveness [3–7].

The storage of electric charges in activated carbons is mainly non-Faradaic, and the accumulation of ionic charges occurs on a double layer at the electrode/electrolyte interface [1]. The large specific surface area and the porosity of activated carbons are the basic requirements to achieve the quick formation of a double layer, the capacitive behaviors of activated carbons are influenced by their exposed surface area and pore size distribution. In addition, most of activated carbons have the functional groups containing many heteroatoms (such as oxygen, nitrogen, sulfur, and halogen) with a certain fraction, due to the residual surface-valence of carbons. The presence of these functionalities gives activated carbons an acid-base character [8–10], which enhances their capacitance by the pseudocapacitive effect [1]. Therefore, tailoring porous structure and surface chemistry of activated carbons is very important to improve electrochemical performance of supercapacitors [11–17].

Activated carbons can be prepared by physical and chemical activation methods and, occasionally, by combination of both types of methods. Physical activation is a two-step procedure: carbonization under inert atmosphere, followed by controlled gasification of the char with suitable oxidizing agents such as air, steam,

or CO_2 at temperatures in the 350–550 °C range (air) and between 800 and 1,100 °C (steam and CO_2) [18]. Chemical activation is the process where carbonization and activation of a precursor material occur simultaneously in the presence of dehydrating chemicals (i.e., H_3PO_4, $ZnCl_2$, H_2SO_4, and KOH), which influence the course of the pyrolysis, between 400 and 800 °C [18]. The great advantage of chemical activation is that it demands less consumption of energy than physical activation because there is only one calcination step, and it is made at lower temperature [19].

Polyaniline (PANI) contains about 15 wt.% of nitrogen and 79 wt.% of carbon, which is commercially available and very cheap, so we believe that it is a promising nitrogen-containing carbon material for supercapacitors. Previously, we have prepared a doped activated carbon from PANI by physical activation [20], it has high performance as an electrode material for supercapacitor, but its specific surface area is low (514 $m^2\ g^{-1}$). We hope to improve its capacitive performance through increasing its specific surface area, so in this paper we have prepared a doped activated carbon with a high specific surface area from PANI by chemical activation with KOH. The comparison of doped unactivated carbon, doped activated carbon prepared by KOH activation and doped activated carbon prepared by physical activation on physical structures and electrochemical characteristics has been deeply investigated.

Experimental

Preparation of PANI base

PANI was prepared by the oxidation of a solution of 20 ml of aniline in 43 ml of 6 mol L^{-1} H_2SO_4 with 20 ml of $(NH_4)_2S_2O_8$ saturated solution. The detailed synthesis route can be found in our previous paper [20]. The PANI obtained from the polymerization was added to excess of 1 mol L^{-1} ammonia solution, then the reaction was kept for 12 h at room temperature under vigorous stirring. Finally, the resulting PANI base was filtered out, washed, and dried at 100 °C for 48 h under vacuum condition.

Preparation of carbon materials

The PANI base was soaked with a 2.0 wt.% KOH solution under vigorous stirring for 2 h, and then it was dried at 105 °C until a constant weight was reached, the weight ratio of PANI base to KOH was 2:1. For activation, the sample was transferred into a graphite crucible and was heated to 700 °C at a heating rate of 7 °C min^{-1} under nitrogen flow and maintained at the desired temperature for 2 h. The KOH activation process may be as follows [21]:

$$\mathrm{PANI} \xrightarrow[700^{\circ}\mathrm{C}]{\text{carbonization}} \mathrm{C} \quad (1)$$

$$4\mathrm{KOH} + \mathrm{C} \rightarrow \mathrm{K_2CO_3} + \mathrm{K_2O} + 3\mathrm{H_2} \quad (2)$$

$$\mathrm{K_2O} + \mathrm{C} \rightarrow 2\mathrm{K} + \mathrm{CO} \quad (3)$$

$$\mathrm{K_2CO_3} + 2\mathrm{C} \rightarrow 2\mathrm{K} + 3\mathrm{CO} \quad (4)$$

The resulting doped activated carbon was cooled to room temperature under ambient condition, and then was washed with a 0.5 mol L^{-1} HCl solution. Subsequently, the sample was repeatedly washed with hot distilled water until the pH of solution reached 6–7. Finally, the sample was dried at 100 °C for 24 h under vacuum condition. The obtained doped activated carbon was marked as CKA700. For comparison, a carbonized sample was prepared from PANI base without KOH. The preparative procedure was the same as that of CKA700, the carbonized sample was marked as C700. Another doped activated carbon (CA800) was used as comparison, its preparation process is simply as follows: first, PANI was prepared by the polymerization of aniline; second, the as prepared PANI was carbonized at 800 °C for 2 h; finally, the obtained carbon was activated at 400 °C for 2 h in the mixed gas of O_2 and N_2 (the volume percent of O_2 is 5%). the detailed preparation and some experimental data of CA800 can be found in our previous paper [20].

The characterization of materials

Scanning electron microscope (SEM) measurements were performed on a Hitachi S5200 scanning electron microscope. The nitrogen adsorption–desorption isotherms of the samples at 77 K were measured by an automatic adsorption instrument (Quantachrome Inst., NOVA-2200). The specific surface areas and average pore diameters were calculated by Brunauer–Emmett–Teller (BET) equation. The pore size distribution was estimated by Barrett–Joyner–Halenda (BJH) method. The surface chemical composition of the samples was determined by X-ray photoelectron spectroscopy (XPS) using a VG Scientific ESCALAB 250 spectrometer with an Al Kα source. The sample charge was corrected using the C1s peak (284.6 eV) as an internal standard. A non-linear, Shirley-type baseline and an iterative least-squares fitting algorithm were used to decompose the peaks. The surface atomic ratios were calculated from the ratio of the

corresponding peak areas after correction with the theoretical sensitivity factors based on the Scofield's photoionization cross-sections.

Electrochemical testing

The capacitive performances of all samples were evaluated in 6 mol L^{-1} aqueous KOH using two-electrode testing cells. The working electrode was prepared by mixing the carbon sample with acetylene black and polyvinylidene fluoride in *N*-methyl-2-pyrrrolidone at a ratio of 8:1:1. The homogeneous slurry was coated on a nickel foil (current collector) with a total surface area of active material of 4 cm^2. The electrodes were dried at 100 °C for 12 h and then weighed. Two electrodes with identical or very close masses were selected and then assembled as supercapacitors. Cyclic voltammograms (CV) were recorded from 0 to 1 V at various sweep rates, galvanostatic charge/discharge curves were recorded from 0 to 1 V loading different current densities and electrochemical impedance spectroscopy measurements were carried out by applying an AC voltage of 5 mV amplitude in the 100 kHz–10 mHz frequency range using a CHI 660A electrochemical workstation (CHI Inc., USA). All electrochemical measurements were carried out at room temperature.

The specific gravimetric capacitance of the electrode is obtained from the Eq. 5:

$$C_g = \frac{I\Delta t}{m\Delta V} \times 2 \tag{5}$$

where C_g (F g^{-1}) is the specific gravimetric capacitance, I (A) is the current loaded, Δt(s) is the discharge time, ΔV (V) is the potential change during the discharge process (1 V in this study), and m (g) represents the mass of electroactive material.

Results and discussion

Characteristics of the carbon samples

Figure 1a depicts the representative SEM image of C700, it is with a lot of large particles stacking together. From the SEM image of CKA700 (Fig. 1b), a lot of pores can be clearly observed, it is because the chemical reactions between KOH and carbon occurred during the activation process and it played an important role in the development of the porosity of the activated carbon [21].

The N_2 adsorption–desorption isotherms as shown in Fig. 2a, were used to determine the surface area and pore size distribution of the C700, CKA700, and CA800. In the isotherm of C700, the adsorbed volume is very small, indicating its nonporous characteristic. The isotherm of CA800 exhibits type I of the IUPAC classification, which shows a well-defined plateau, it confirms its microporosity. However, the isotherm of CKA700 is type I mixed with type IV, which shows a typical hysteresis loop. In low relative pressure range, high adsorption of N_2 occurred, while an obvious capillary condensation step (hysteresis loop) was detected from the relative pressure (P/P_0) of 0.45 to 0.97, indicating the presence of both micropores and mesopores [22]. The N_2 adsorbed below P/P_0=0.02 may be attributed to the micropore filling. The N_2 uptake at $P/P_0 = 0.02 - 0.2$ can be easily observed from the isotherm of CKA700, suggesting the presence of supermicropores and small mesopores. The isotherm of CKA700 also exhibited some limited N_2 uptake at P/P_0>0.2, which may be attributed to adsorption into mesopores [23].

Figure 2b denotes the pore size distributions of CA800 and CKA700 with BJH method. As is shown in Fig. 2b, peaks at pore diameter less than 2 nm indicate the formation of micropores in both CA800 and CKA700. However, it is noticed that there exists the second sharp peak in the pore diameter about 3.8 nm on the curve of

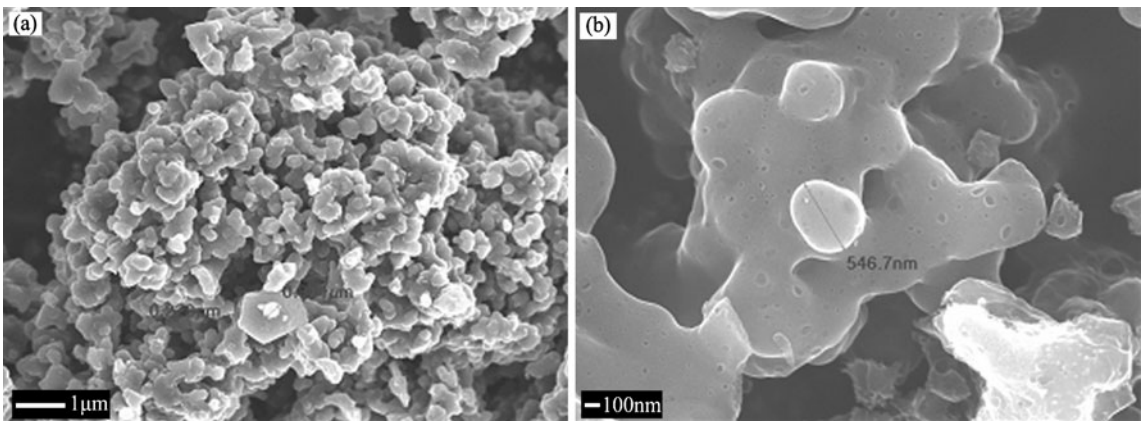

Fig. 1 SEM images of **a** C700 and **b** CKA700

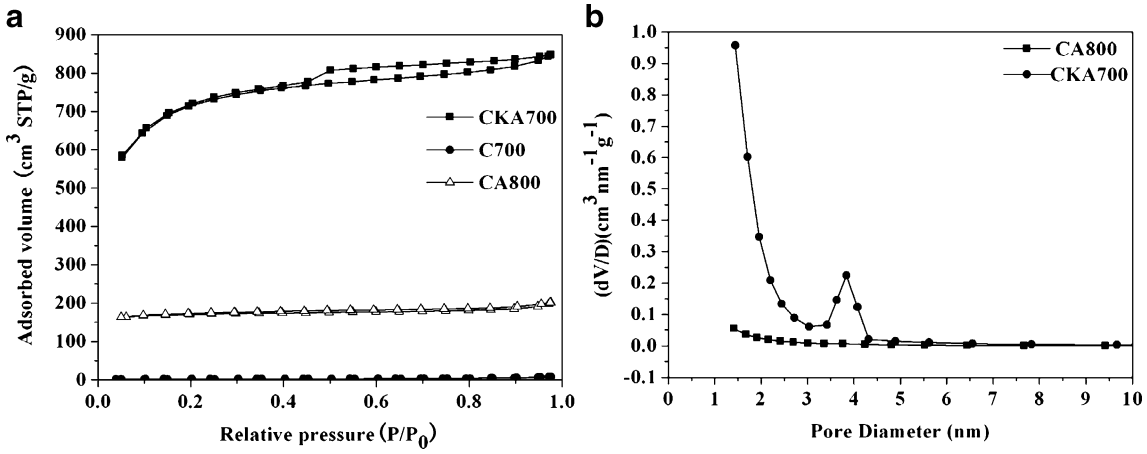

Fig. 2 N_2 adsorption/desorption isotherms (**a**) and the pore size distributions (**b**) of the samples. The pore size distribution is calculated using adsorption branch by the BJH method

CKA700, which confirms that CKA700 contains both micropore and mesopore structure.

Table 1 summarizes the textural properties of the samples. C700 possesses very low surface area (9 $m^2\ g^{-1}$) because of its nonporous characteristic, however, the surface area of CKA700 increases sharply through KOH activation, with its value being as high as 2,287 $m^2\ g^{-1}$, which is nearly four times as much as that of CA800 (514 $m^2\ g^{-1}$). Babel et al. [24] got an activated carbon produced from lignin processed by standard carbonization and KOH activation, the surface area is 1,946 $m^2\ g^{-1}$; Kim et al. [25] prepared nitrogen-enriched carbon materials from peptides of silk fibroins with KOH activation, its surface area was as high as 2,612 $m^2\ g^{-1}$, it was clear that KOH activation was an effect method to improve the surface area of carbon samples. The total pore volume of CKA700 is much higher than that of CA800, and the average pore diameter of CKA700 is also higher than that of CA800, it is because CKA700 has both micropores and mesopores.

The XPS spectra of the three carbons indicate the presence of three distinct peaks, which can be explained by existence of carbon, nitrogen, and oxygen atoms. The XPS spectra of CA800 have been published previously [20], and therefore, Fig. 3 displays only that of C700 and CKA700. Fitting of the C1s spectrum can be resolved into four individual component peaks representing graphitic carbon (Peak 1, $BE = 284.6 - 285.1$ eV), carbon present in alcohol or ether groups (Peak 2, $BE = 286.3 - 287.0$ eV), carbonyl groups (Peak 3, $BE = 287.5 - 288.1$ eV), and carboxyl or ester groups (Peak 4, $BE = 289.3 - 290.0$ eV) [26]. Various oxygen-containing functional groups existing on the carbon surface are also confirmed through XPS measurement. O1s core level spectrum reveals the presence of five peaks, corresponding to C=O groups (530.9 eV), carbonyl oxygen atoms in esters, amides, anhydrides, and oxygen atoms in hydroxyls or ethers (532.2 eV), the ether oxygen atoms in esters and anhydrides (533.3 eV), and the oxygen atoms in carboxyl groups (534.5 eV) and chemisorbed water (536.1 eV) [27, 28].

To understand the role of nitrogen functionalities in capacitive performance, it is necessary to clarify the types of nitrogen introduced onto the carbon surface. According to the literatures [29–32], the chemical state of nitrogen atoms in graphene structure could be assigned to four types: N-6 (pyridinic nitrogen, 398.7±0.3 eV), N-5 (pyrrolic nitrogen and pyridone nitrogen in association with oxygen functionality, 400.3±0.3 eV), N-Q (quaternary nitrogen, nitrogen substituted with carbons in the aromatic grapheme structure, 401.4±0.5 eV), and N-X (pyridine -*N*-oxide, 402–405 eV). Except for the N-Q, all nitrogen functionalities are located at the edges of graphene layers. The locations of nitrogen functionalities within the carbon matrix are schematically displayed in Fig. 4. The peak analyses of N1s for the three samples reveal the presence of the same four contributions, but with different relative contributions. The proportion of pyridinic, pyrrolic, quaternary, and oxidized nitrogen of the three samples and the atomic concentration of them are summarized in Table 2. As is shown, the nitrogen content of C700 is the highest (12.16%), that of CA800 (10.89%) decreases slightly, but

Table 1 Textural characteristics and specific capacitance of C700, CA800, and CKA700

Sample	S_{BET}	L_0	V_T	C_g
C700	9	–	–	75
CKA700	2,287	1.443	0.850	220
CA800	514	1.417	0.189	235

S_{BET} BET surface area ($m^2\ g^{-1}$), L_0 average pore diameter (nm), V_T total pore volume ($cm^3\ g^{-1}$), C_g specific gravimetric capacitance at the current density of 0.5 A g^{-1} (F g^{-1})

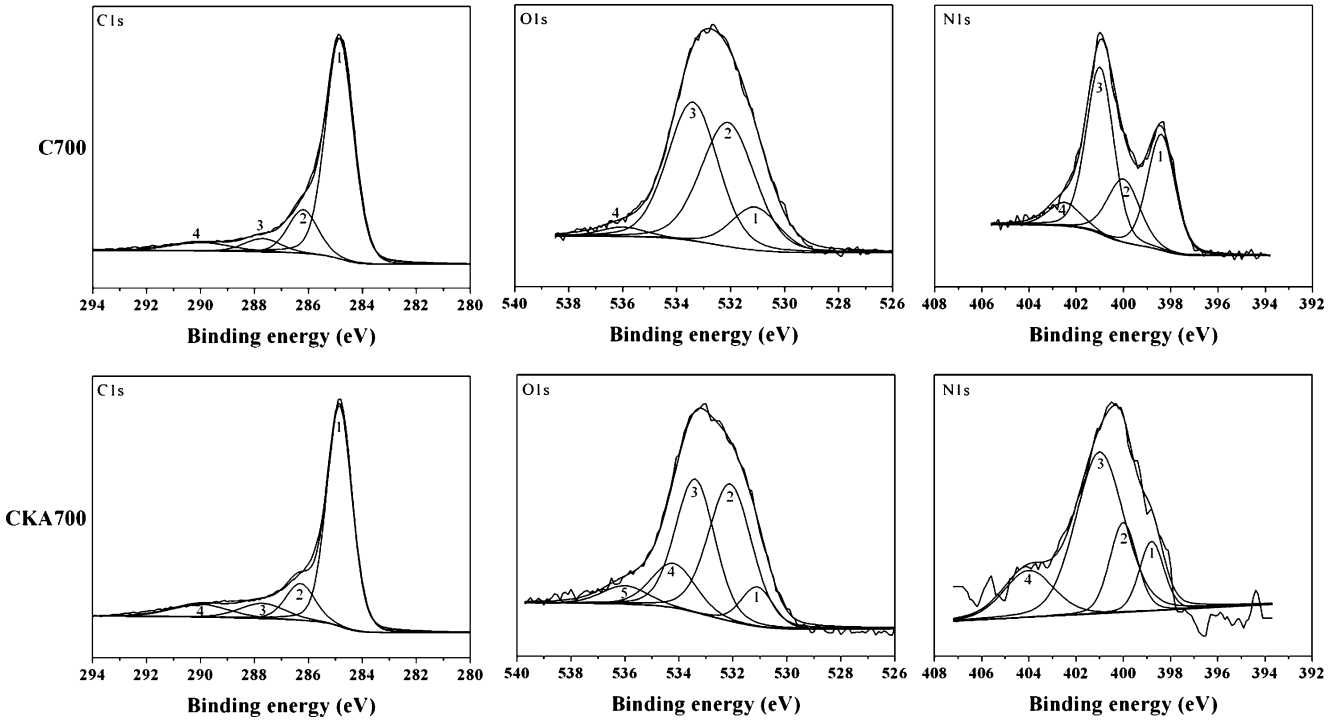

Fig. 3 X-ray photoelectron spectra of C700 and CKA700

that of CKA700 (3.72%) decreases sharply, the reason may be that nitrogen functionalities within the carbon matrix can react with KOH to generate nitrogen oxides in high temperature. The peak deconvolution analysis shows that the content of pyridinic and pyrrolic nitrogen in nitrogen functionalities of C700, CKA700, and CA800 is 49.6%, 29.1%, and 86.5%, respectively. Pyrrolic nitrogen, which improves the charge mobility in a carbon matrix by introducing electron-donor characteristics and enhancing the carbon catalytic activity in electron-transfer reactions, is an electrochemically active nitrogen; the pyridinic nitrogen, which can also provide a lone electron pair for conjugation with the π-conjugated rings, is also an electrochemically active nitrogen, so the pseudocapacitance is mainly induced by pyridinic and pyrrolic nitrogen [33].

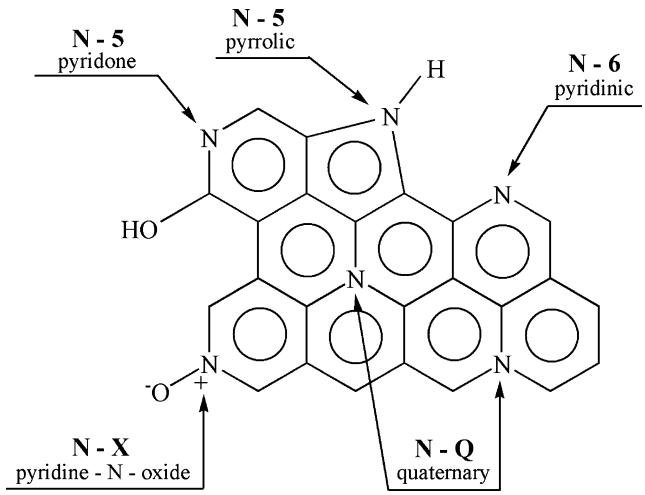

Fig. 4 Schematic model of the carbon matrix, indicating the locations of the various nitrogen-containing functional groups

Electrochemical properties of carbon electrodes

CV was used in determination of electrochemical properties of as-prepared samples. Figure 5a shows the CV plots of three samples at a sweep rate of 2 mV s^{-1} with the potential range of 0 to 1 V. At this sweep rate all CV curves exhibit near rectangular shapes, which is the characteristic of electrochemical capacitor. The range of current density of CKA700 is much higher than that of C700, which indicates CKA700 has much higher specific capacitance than C700. But compared to CA800, the CV curve of CKA700 exhibits a little smaller current response and area of rectangle, suggesting CKA700 has a little lower specific capacitance than CA800. The CV plots of the CKA700 at different sweep rates are shown in Fig. 5b. At 2, 5, and 10 mV s^{-1}, the curves present the typical rectangle "box-like" shape for charge/discharge process. At higher scan rates, for example, at 20 mV s^{-1}, the shape of the curve is still satisfactory, which indicates quick dynamics of charge propagation with this kind of carbon. The above results also suggest that CKA700 may be a promising candidate for supercapacitors.

Table 2 Surface composition and nitrogen form distribution in C700, CA800, and CKA700

Sample	Atomic concentration				Nitrogen form distribution				
	C	N	O	N_1[a]	N-6	N-5	N-Q	N-X	(N−6 + N−5)
C700	76.21	12.16	7.46	6.03	30.2	19.4	43.1	7.3	49.6
CKA700	86.55	3.72	9.73	1.08	12.0	17.1	54.4	16.5	29.1
CA800	80.98	10.89	8.13	9.42	37.40	49.1	9.6	3.9	86.5

[a] The content of N-6 and N-5 of the samples

The galvanostatic charge/discharge curves at a loading current density of 0.5 A g^{-1} for three carbons are shown in Fig. 6. The charge/discharge profile of C700 exhibits an obvious ohmic drop, indicating that it possesses a bad capacitive behavior, the specific capacitance of C700 is small, just 75 F g^{-1} (see Table 1), it is because the surface area of C700 is very small (9 m^2 g^{-1}), it is clear that the contribution of the double-layer capacitance to the overall capacitance is negligible, the overall capacitance mainly arises from pseudocapacitance afforded by nitrogen functionalities. However, both CKA700 and CA800 present isosceles triangle charge/discharge curves without obvious ohmic drop, indicating that both of them possess a good capacitive behavior under this loading current density. The surface area of CKA700 is nearly four times than that of CA800 (see Table 1), but the specific capacitance of CKA700 is 220 F g^{-1}, a little smaller than that of CA800 (235 F g^{-1}, see Table 1). There is no linear relationship between specific capacitance and surface area, which is because the overall specific capacitance consists of pseudocapacitance and double-layer capacitance. Compared to CA800, the surface area of CKA700 increases significantly, but the nitrogen content of CKA700 decreases significantly (3.72%) and the content of pyridinic and pyrrolic nitrogen in all nitrogen functionalities decreases clearly (29.1%, see Table 2), the content of pyridinic and pyrrolic nitrogen of CKA700 is only 1.08%, we have known that the pseudocapacitance is mainly induced by pyridinic and pyrrolic nitrogen [33], so the pseudocapacitance becomes very small and can be negligible, the overall specific capacitance of CKA700 is mainly attributed to double-layer capacitance. However, the content of pyridinic and pyrrolic nitrogen of CA800 is 9.42%, which can provide more pseudocapacitance, and CA800 has moderate specific surface area which can provide some double-layer capacitance, the overall specific capacitance of CA800 is attributed to the synergic effect of pseudocapacitance and double-layer capacitance. So the overall specific capacitance of CKA700 does not increase significantly because of specific surface area increasing significantly.

In order to understand the impedance performance clearly, Nyquist plot of all the carbon samples are shown in Fig. 7. As is shown in Fig. 7a, a very big semicircle in the middle and high-frequency region is observed from C700, suggesting C700 has a very big intrinsic resistance, but after activation, the semicircles become very small from CKA700 and CA800, suggesting they have small intrinsic resistance, it may be attributed to the porous characteristic. At the very high-frequency region, the intercept at the real axis is the equivalent series resistance. From Fig. 7b, we can know that the equivalent series resistance values of C700, CKA700, and CA800 are 1.65, 1.39, and 0.75 Ω, respectively, indicating that the electric conductivity gradually increases. Compared to C700, the equivalent series

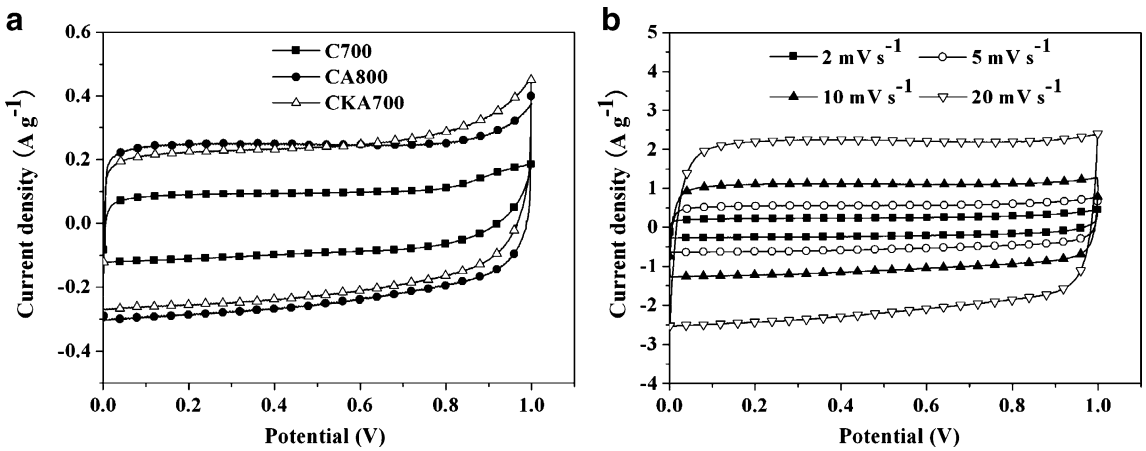

Fig. 5 Cyclic voltammograms of carbon electrodes in 6 mol L^{-1} KOH electrolyte: **a** C700, CA800, and CKA700 at a scan rate of 2 mV s^{-1}, **b** CKA700 with different scan rates

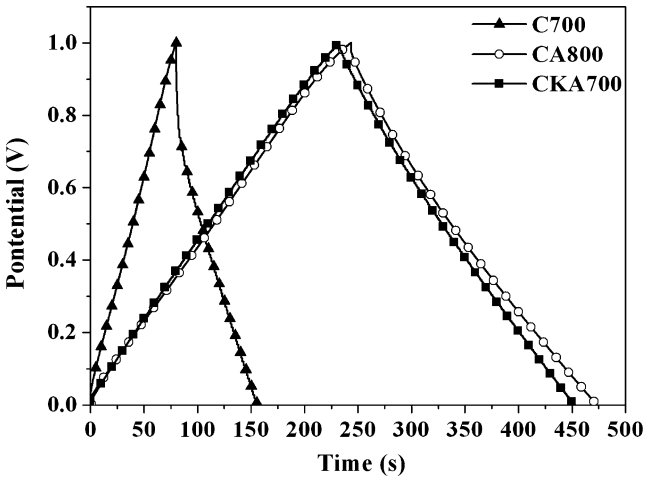

Fig. 6 Charge/discharge curves of C700, CA800, and CKA700 at the current density of 0.5 A g^{-1}

resistance value of CKA700 decreases, the reason may be that the carbon after activation generates a number of polar groups which result in the increase of the electric conductivity [20]. However, compared to CA800, the equivalent series resistance value of CKA700 clearly increases, which is attributed to the very high surface area (see Table 1) and very low nitrogen content (see Table 2), because the electrical conductivity of porous carbon decreases with increasing porosity owing to the non-compatibility of the conductive pathways [33], while nitrogen functionalities can enhance the surface wettability and reduce the resistance of carbon [11]. The surface area of CKA700 is much higher than that of CA800 and the nitrogen content of CKA700 is much lower than that of CA800, so the electrical conductivity of CKA700 is much lower than that of CA800. The imaginary part of the impedance spectra at low-frequency region represents the capacitive behavior of the electrode and approaches a 90° vertical line in an ideal capacitor [1]. Obviously, compared to C700, the straight line part of CKA700 is more close to vertical line along the imaginary axis, suggesting CKA700 has better capacitive behavior than C700, but CKA700 and CA800 have almost the same good capacitive behavior.

Conclusions

Doped carbons have been prepared from polyaniline as supercapacitors, their charge storage performance has been evaluated by various techniques. The effect of nitrogen atomic functionalities on the pseudocapacitive property has been studied. Compared to C700, the specific surface area and specific capacitance of CKA700 increase significantly; compared to CA800, its specific surface area increases significantly, but all its nitrogen content decreases significantly, especially the content of pyridinic and pyrrolic nitrogen. Two kinds of capacitance contribution are involved in the doped carbons: one kind is double-layer capacitance coming from the formation of the electrical double layer, the other is pseudocapacitance induced by nitrogen functionalities, especially pyridinic and pyrrolic nitrogen. So the overall specific capacitance of CA800 is attributed to the synergic effect of pseudocapacitance and double-layer capacitance, but the pseudocapacitance of CKA700 becomes very small, so the overall specific capacitance of CKA700 is mainly attributed to double-layer capacitance. Although these electrochemical characteristics testify that CKA700 may be a promising candidate for supercapacitors, further investigations are necessary on the preparation of doped activated carbons whose specific surface area can significantly increase, at the same time, whose nitrogen functionalities, particularly pyridinic and pyrrolic nitrogen can be held richly, in order to obtain doped activated carbon whose specific capacitance can further increase.

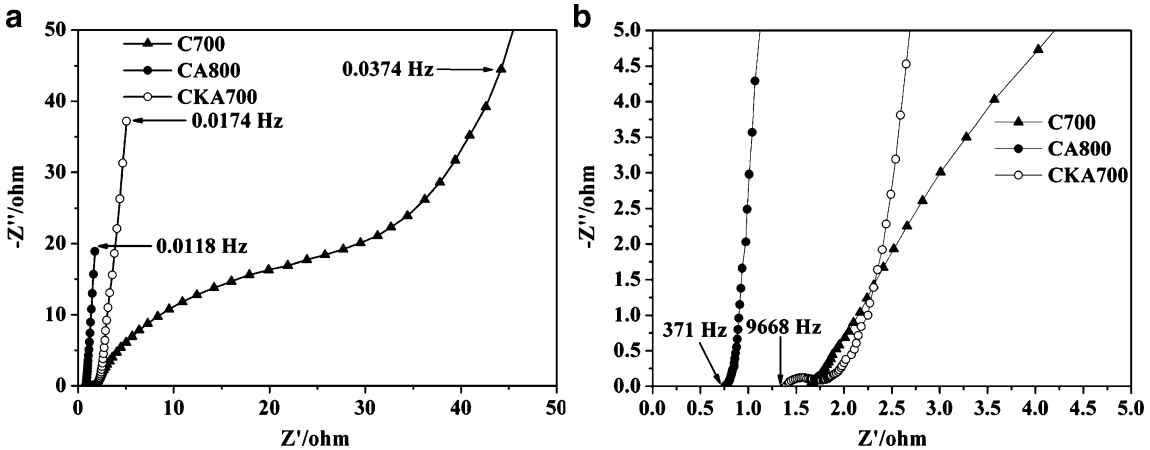

Fig. 7 Nyquist plot of **a** C700, CA800, and CKA700, **b** enlarged high-frequency region of Nyquist plot

Acknowledgment The authors are grateful for Project supported by Hunan Provincial Natural Science Foundation of China (07JJ6015).

References

1. Conway BE (1999) Electrochemical supercapacitors—scientific fundamentals and technological applications. Kluwer Academic/ Plenum, New York
2. Winter M, Brodd RJ (2004) Chem Rev 104:4245
3. Xu B, Wu F, Chen S, Zhou ZM, Cao GP, Yang YS (2009) Electrochim Acta 54:2185
4. Ruiz V, Santamaría R, Granda M, Blanco C (2009) Electrochim Acta 54:4481
5. Lin YC, Wu SH, Liu CW, Lim ZY, Huang CW, Lin HP, Deng S, Yang MC, Tang CY, Lin CY (2008) J Solid State Electrochem 12:895
6. Lätt M, Käärik M, Permann L, Kuura H, Arulepp M, Leis J (2010) J Solid State Electrochem 14:543
7. Zhang GQ, Zhang ST (2009) J Solid State Electrochem 13:887
8. Li WR, Chen DH, Li Z, Shi YF, Wan Y, Huang JJ, Yang JJ, Zhao DY, Jiang ZY (2007) Electrochem Commun 9:569
9. Hulicova-Jurcakova D, Seredych M, Lu GQ, Kodiweera NKAC, Stallworth PE, Greenbaum S, Bandosz TJ (2009) Carbon 47:1576
10. Sepehri S, García BB, Zhang QF, Cao GZ (2009) Carbon 47:1436
11. Li WR, Chen DH, Li Z, Shi YF, Wan Y, Wang G, Jiang ZY, Zhao DY (2007) Carbon 45:1757
12. Ania CO, Khomenko V, Raymundo-Piñero E, Parra JB, Béguin F (2007) Adv Funct Mater 17:1828
13. Chang KW, Lim ZY, Du FY, Yang YL, Chang CH, Hu CC, Lin HP (2009) Diamond Relat Mater 18:448
14. Raymundo-Piñero E, Leroux F, Béguin F (2006) Adv Mater 18:1877
15. Kim W, Joo JB, Kim N, Oh S, Kim P, Yi J (2009) Carbon 47:1407
16. Xu B, Wu F, Chen RJ, Cao GP, Chen S, Zhou ZM, Yang YS (2008) Electrochem Commun 10:795
17. Ra EJ, Raymundo-Piñero E, Lee YH, Béguin F (2009) Carbon 47:2984
18. Olivares-Marín M, Fernández-González C, Macías-García A, Gómez-Serrano V (2006) Appl Surf Sci 252:5980
19. Cardoso B, Mestre AS, Carvalho AP, Pires J (2008) Ind Eng Chem Res 47:5841
20. Li LM, Liu EH, Li J, Yang YJ, Shen HJ, Huang ZZ, Xiang XX, Li W (2010) J Power Sources 195:1516
21. Lu CL, Xu SP, Gan YX, Liu SQ, Liu CH (2005) Carbon 43:2295
22. Kruk M, Jaroniec M (2001) Chem Mater 13:3169
23. Yang ZX, Xia YD, Sun XZ, Mokaya R (2006) J Phys Chem B 110:18424
24. Babel K, Jurewicz K (2008) Carbon 46:1948
25. Kim YJ, Abe Y, Yanagiura T, Park KC, Shimizu M, Iwazaki T, Nakagawa S, Endo M, Dresselhaus MS (2007) Carbon 45:2116
26. Biniak S, Szymański G, Siedlewski J, Światkowski A (1997) Carbon 35:1799
27. Zielke U, Hüttinger KJ, Hoffman WP (1996) Carbon 34:983
28. Figueiredo JL, Pereira MFR, Freitas MMA, Órfão JJM (1999) Carbon 37:1379
29. Kapteijn F, Moulijn JA, Matzner S, Boehm HP (1999) Carbon 37:1143
30. Bagreev A, Menendez JA, Dukhno I, Tarasenko Y, Bandosz TJ (2004) Carbon 42:469
31. Jurewicz K, Babel K, Ziolkowski A, Wachowska H (2003) Electrochim Acta 48:1491
32. Jurewicz K, Babel K, Ziolkowski A, Wachowska H (2004) J Phys Chem Solids 65:269
33. Hulicova-Jurcakova D, Kodama M, Shiraishi S, Hatori H, Zhu ZH, Lu GQ (2009) Adv Funct Mater 19:1800